Volatile chemical product emissions enhance ozone and modulate urban chemistry

Matthew M. Coggon[a,b,1], Georgios I. Gkatzelis[a,b], Brian C. McDonald[b], Jessica B. Gilman[b], Rebecca H. Schwantes[a,b], Nader Abuhassan[c], Kenneth C. Aikin[a,b], Mark F. Arend[d,e], Timothy A. Berkoff[f], Steven S. Brown[b], Teresa L. Campos[g], Russell R. Dickerson[h], Guillaume Gronoff[f], James F. Hurley[i], Gabriel Isaacman-VanWertz[i], Abigail R. Koss[j], Meng Li[a,b], Stuart A. McKeen[a,b], Fred Moshary[d,e], Jeff Peischl[a,b], Veronika Pospisilova[j], Xinrong Ren[h,k], Anna Wilson[l], Yonghua Wu[d,e], Michael Trainer[a,b], and Carsten Warneke[a,b]

[a]Cooperative Institute for Research in Environmental Sciences, University of Colorado, Boulder, CO 80309; [b]Chemical Sciences Laboratory, National Oceanic and Atmospheric Administration, Boulder, CO 80305; [c]Joint Center for Earth Systems Technology, University of Maryland Baltimore County, Baltimore, MD 21250; [d]National Oceanic and Atmospheric Administration Cooperative Science Center for Earth System Sciences and Remote Sensing Technologies, The City College of New York, New York, NY 10031; [e]Department of Electrical Engineering, The City College of New York, New York, NY 10031; [f]Langley Research Center, National Space and Aeronautical Administration, Hampton, VA 23666; [g]Atmospheric Chemistry Observations and Modeling Laboratory, National Center for Atmospheric Research, Boulder, CO 80305; [h]Department of Atmospheric and Oceanic Science, University of Maryland, College Park, MD 20742; [i]Department of Civil and Environmental Engineering, Virginia Polytechnic Institute and State University, Blacksburg, VA 24061; [j]Tofwerk AG, 3600 Thun, Switzerland; [k]Air Resources Laboratory, National Oceanic and Atmospheric Administration, College Park, MD 20740; and [l]Department of Chemical and Petroleum Engineering, University of Kansas, Lawrence, KS 66045

Edited by Veerabhadran Ramanathan, University of California San Diego, La Jolla, CA, and approved June 10, 2021 (received for review December 28, 2020)

Decades of air quality improvements have substantially reduced the motor vehicle emissions of volatile organic compounds (VOCs). Today, volatile chemical products (VCPs) are responsible for half of the petrochemical VOCs emitted in major urban areas. We show that VCP emissions are ubiquitous in US and European cities and scale with population density. We report significant VCP emissions for New York City (NYC), including a monoterpene flux of 14.7 to 24.4 kg · d^{-1} · km^{-2} from fragranced VCPs and other anthropogenic sources, which is comparable to that of a summertime forest. Photochemical modeling of an extreme heat event, with ozone well in excess of US standards, illustrates the significant impact of VCPs on air quality. In the most populated regions of NYC, ozone was sensitive to anthropogenic VOCs (AVOCs), even in the presence of biogenic sources. Within this VOC-sensitive regime, AVOCs contributed upwards of ∼20 ppb to maximum 8-h average ozone. VCPs accounted for more than 50% of this total AVOC contribution. Emissions from fragranced VCPs, including personal care and cleaning products, account for at least 50% of the ozone attributed to VCPs. We show that model simulations of ozone depend foremost on the magnitude of VCP emissions and that the addition of oxygenated VCP chemistry impacts simulations of key atmospheric oxidation products. NYC is a case study for developed megacities, and the impacts of VCPs on local ozone are likely similar for other major urban regions across North America or Europe.

volatile chemical products | urban atmospheric chemistry | air pollution | ozone

Regulations of motor vehicle emissions have resulted in decades of declining mixing ratios of nitrogen oxides (NO_x) (1, 2) and volatile organic compounds (VOCs) (3) in US urban areas, which has significantly reduced regional ozone pollution. Despite revisions to the US National Ambient Air Quality Standards (NAAQS) and continued efforts to decrease NO_x and VOC emissions from motor vehicles, reductions in ozone pollution have slowed in recent years. A variety of explanations has been offered for this slowdown, including a shift away from the dominance of combustion sources toward a pollution mixture that includes noncombustion sources (2, 4), increasing levels of global atmospheric ozone (5), and nonlinearities in chemical regimes that influence ozone production efficiency (6).

Recent work in Los Angeles, CA, has shown that emissions from consumer and industrial products (collectively "volatile chemical products," VCPs) now contribute as much as 50% to total petrochemical VOCs in major urban areas (4) and as much as 10 ppb to urban ozone (7). In smaller cities, consumer product usage has been shown to be a significant source of urban VOCs, as evidenced by emissions of the personal care product tracer decamethylcyclopentasiloxane (D5-siloxane) (8). By leveraging advances in analytical instrumentation now capable of detecting VOC tracers linked to VCP emissions, we show that VCPs are ubiquitous in US and European cities and that urban-scale VCP emission fluxes can outweigh biogenic and fossil fuel sources, depending on population density. We show that VCPs contribute significantly to the formation of ozone and other secondary products and that additional chemical reactions are needed in air quality models in order to capture the atmospheric chemistry of VCPs. Furthermore, we show that anthropogenic VOC (AVOC) reduction along with NO_x controls may be a complementary

Significance

Recent work in Los Angeles has shown that urban volatile organic compound (VOC) emissions from consumer and industrial products—termed volatile chemical products (VCPs)—are now an important source of ozone precursors. Using advancements in VOC instrumentation, we show that VCP emissions are ubiquitous in urban regions and can be identified via unique VOC fingerprints. Through detailed modeling, we show that VCPs are as important to ozone production as fossil fuel VOCs and that the chemistry of VCPs can have significant impacts on model simulations of key atmospheric processes. Consequently, air quality models must be updated to account for both the emissions and atmospheric chemistry of VCPs in order to capture their full impact on urban air quality.

Author contributions: M.M.C., B.C.M., and C.W. designed research; M.M.C., G.I.G., B.C.M., J.B.G., R.H.S., N.A., M.F.A., T.A.B., T.L.C., R.R.D., G.G., J.F.H., G.I.-V., A.R.K., M.L., S.A.M., F.M., J.P., V.P., X.R., A.W., Y.W., and C.W. performed research; K.C.A. contributed new reagents/analytic tools; M.M.C., G.I.G., B.C.M., J.B.G., R.H.S., N.A., M.F.A., T.A.B., T.L.C., R.R.D., G.G., J.F.H., G.I.-V., A.R.K., M.L., S.A.M., F.M., J.P., V.P., X.R., A.W., and Y.W. analyzed data; S.S.B., M.T., and C.W. advised research; and M.M.C., G.I.G., B.C.M., J.B.G., and C.W. wrote the paper.

The authors declare no competing interest.

This article is a PNAS Direct Submission.

[1]To whom correspondence may be addressed. Email: matthew.m.coggon@noaa.gov.

This article contains supporting information online at https://www.pnas.org/lookup/suppl/doi:10.1073/pnas.2026653118/-/DCSupplemental.

Published August 2, 2021.

strategy to further improve air quality, even in regions with strong biogenic emissions such as the Eastern United States.

Results and Discussion

VCP Emissions Observed across US and European Cities. To evaluate the relationship between VCPs, traffic emissions, and urban population, we measured VOCs from a mobile laboratory in US and European cities using a proton transfer reaction time-of-flight mass spectrometer (PTR-ToF-MS) and whole air sampling system. We also measured VOCs in New York City (NYC) from a ground site located at the City College of New York (CCNY) during winter (March 5 to 28, 2018) and summer (July 5 to 24, 2018) to quantify VCP impacts on the air quality of the most densely populated region of the United States. A full description of the measurements and sampling strategy is provided in the *Materials and Methods* and *SI Appendix*.

The consumption of most consumer goods scales with city population across the world (9). Transportation emissions also increase with population (10) but are expected to plateau in large cities because of roadway capacity on vehicle volume (11) and greater use of mass transit (10). Consequently, VCP emissions are expected to increase relative to traffic emissions in more densely populated regions (12). Fig. 1*A* shows the spatial distribution of D5-siloxane mixing ratios across the United States and parts of Europe. D5-siloxane is primarily emitted to the atmosphere from antiperspirants and hair care products and is used as a tracer for emissions from personal care products (8, 13). D5-siloxane mixing ratios are highest in populated regions and generally correlate with population density (e.g., NYC, R^2 = 0.7; Fig. 2).

In Fig. 1*B*, we show urban enhancement ratios (ERs) of D5-siloxane relative to benzene, a marker for gasoline emissions, as measured by mobile laboratories in the United States and parts of Europe. D5-siloxane and benzene are predominantly removed from the atmosphere by reaction with OH and have atmospheric lifetimes of 4 to 6 d under typical OH concentrations (8, 14, 15). On the regional scales considered here, the ratio of these tracers provides constraints on the relative emissions of personal care products versus fossil fuels. We calculate urban ERs for cities sampled during morning hours (Fig. 1*A*, dark blue), when the emissions of D5-siloxane are expected to be highest (8) (see *Materials and Methods* for more details). The ERs for D5-siloxane correlate with population density, supporting the inference that VCP emissions will increase relative to traffic in densely populated regions. We note that the correlation is strongly influenced by the large population of NYC and that additional measurements in other

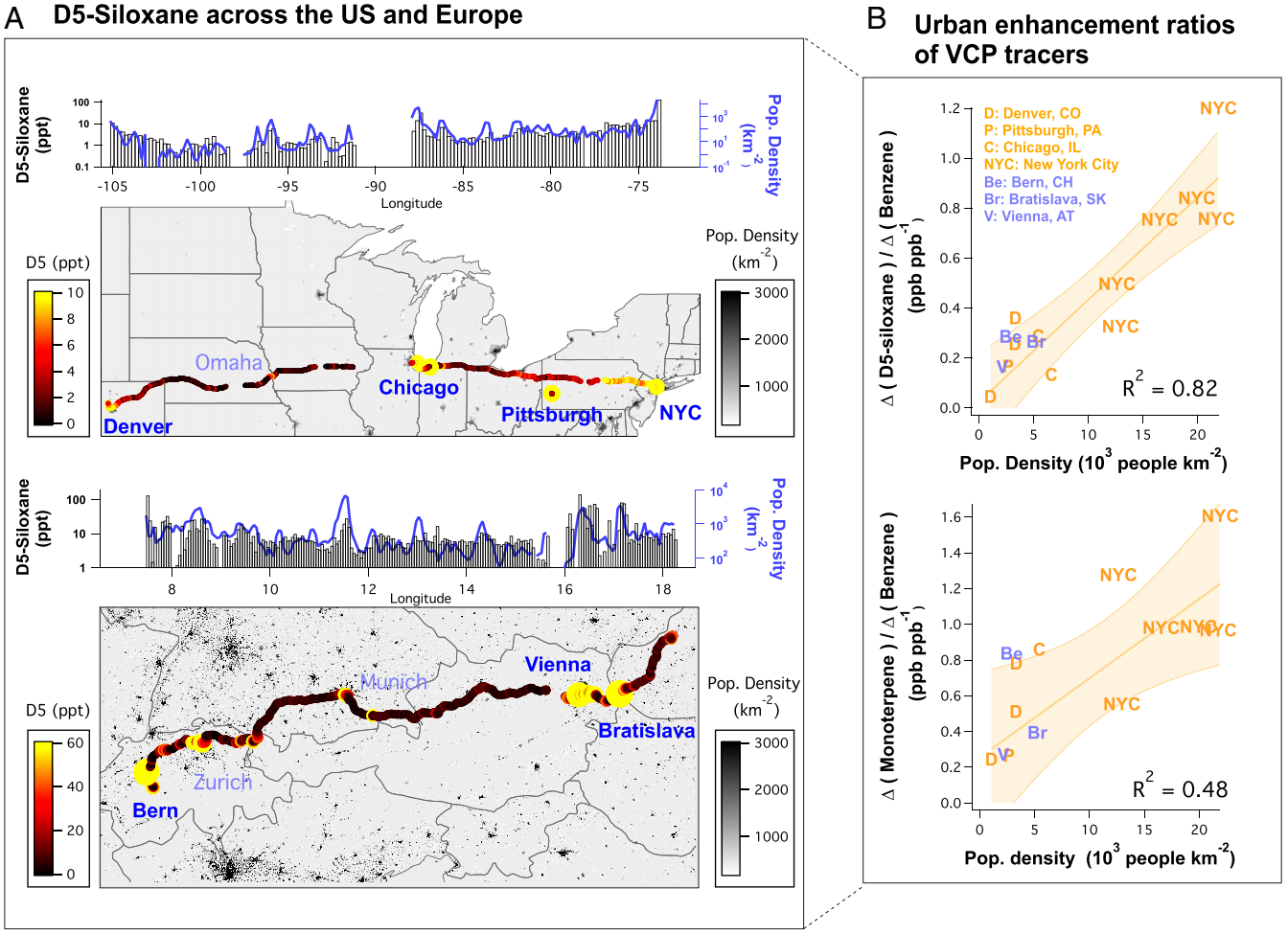

Fig. 1. (*A*) Drive track colored and sized by D5-siloxane measured across the United States and parts of Europe. The distributions above each map show the median mixing ratios of D5-siloxane over longitudinal bins together with the population density within 5 km of the mobile laboratory. (*B*) Relationship between D5-siloxane and monoterpene ERs to benzene (gasoline tracer), with population density for US (orange) and European (blue) cities. The cities presented were sampled during morning hours in densely populated urban centers. For NYC, the data were separated into areas of high, low, and medium population density (see *Materials and Methods*). Error bands represent the 95% CI.

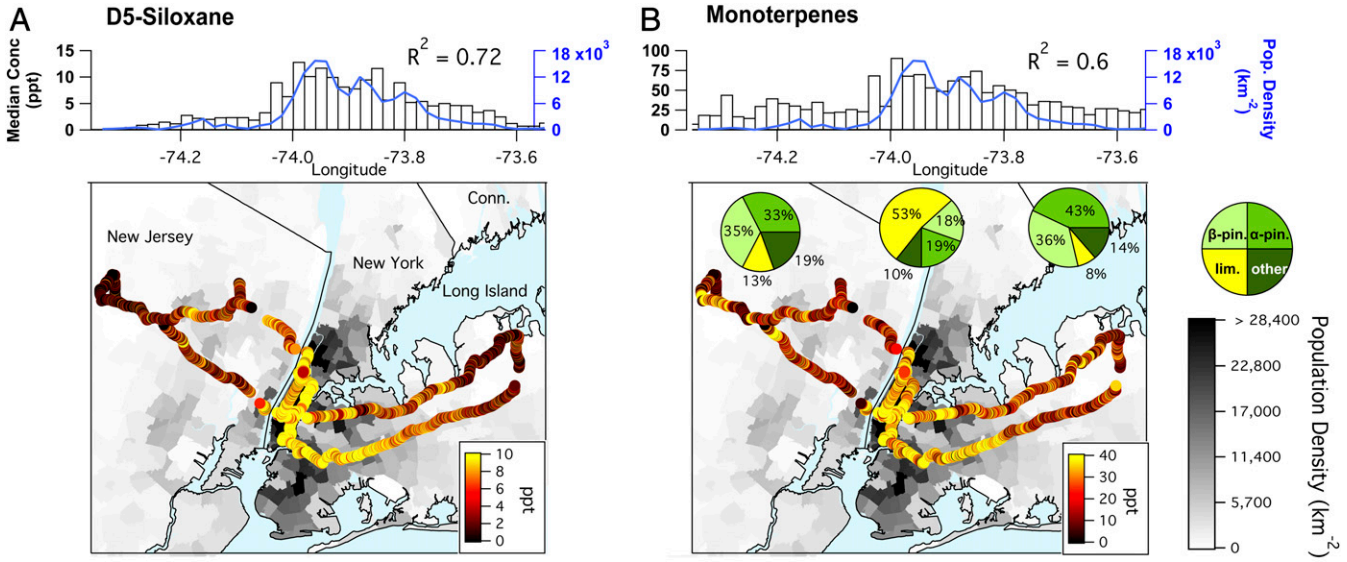

Fig. 2. March 2018 drive tracks colored by D5-siloxane (personal care product tracer) (*A*) and sum of monoterpenes (biogenic + anthropogenic) (*B*) measured by PTR-ToF-MS in winter 2018. Drive tracks overlay a population density map of the NYC region. Pie charts show the composition of monoterpenes measured in (*Left-to-Right*) New Jersey, Manhattan, and Long Island. The distributions above each map show longitudinally binned median mixing ratios of D5-siloxane, median mixing ratios of monoterpenes, and population density along the drive track of the mobile laboratory.

urban regions with intermediate population densities may help to evaluate the robustness of this correlation.

Other VOCs also exhibited this behavior, including ethanol and monoterpenes. Ethanol was the most abundant VOC measured in urban regions (>10 ppb in NYC) to correlate with population density ($R^2 = 0.80$; see *SI Appendix*, section 7 and Fig. S32). Ethanol was previously considered a traffic emission (16) and was only recently linked to emissions from VCPs (4). In NYC, 70% of ethanol is emitted from VCPs and 30% from mobile sources. Monoterpenes are predominantly emitted from biogenic sources during summer months (17); however, in the following sections, we show that emissions from fragranced VCPs are a major source of monoterpenes in urban areas. In contrast to the species described above, carbon monoxide (CO) and aromatic compounds coemitted with benzene from gasoline correlated poorly with population density ($R^2 < 0.11$; *SI Appendix*, Figs. S33 and S34). Gkatzelis et al. (12) evaluates these differences further and concludes that VCPs can be distinguished from fossil fuel sources based on population density proxies.

Fig. 1 demonstrates that VCP emissions impact the VOC burden of cities across the United States and Europe but are most prevalent in dense megacities such as NYC. In the following section, we quantify VOC fluxes in NYC, with a focus on understanding the emissions of anthropogenic monoterpenes from fragranced VCPs.

Monoterpenes in NYC Indicate Significant VCP Emissions. VCP sources emit a wide spectrum of reactive and functionalized VOCs. Fragrances have been studied for their potential air quality impacts on indoor and outdoor air (18–20) and are widely prevalent in personal care and household products (e.g., cleaning products and detergents) (20, 21). A recent industry survey by the California Air Resources Board found that fragrances ranked as one of the top three ingredients listed in consumer products (21). Monoterpenes, especially limonene, are common fragrance ingredients but are traditionally considered to originate from biogenic sources (18, 20). Most monoterpenes are reactive toward ozone, OH, and NO_3 radicals and subject to short atmospheric lifetimes (e.g., 2 h for limonene under typical OH concentrations). Consequently, monoterpenes are likely to have the largest air quality impacts on local scales. Here, we investigate the source and flux of monoterpene emissions to illustrate the significant contribution of fragranced VCPs to the urban VOC burden.

To evaluate the source of monoterpenes in NYC, we compared the spatial profiles of fossil fuel tracers (benzene), combustion tracers (CO), and VCP tracers (D5-siloxane) to the profiles observed for urban monoterpenes. Mobile laboratory measurements show that motor vehicle and combustion emissions are ubiquitous throughout the metropolitan region (*SI Appendix*, Fig. S33). D5-siloxane is primarily enhanced in densely populated areas around Manhattan and is well correlated with population density (Fig. 2*A*, $R^2 > 0.7$). The elevated D5-siloxane mixing ratios and the correlation to population density indicate the significant use of VCPs.

Monoterpene mixing ratios were enhanced in populated regions of NYC during wintertime sampling (Fig. 2*B*), when biogenic monoterpene emissions are expected to be lowest (17). Monoterpenes were highest in downtown NYC and coincident with enhancements in D5-siloxane. Measurements by gas chromatography–mass spectrometry (GC-MS) show limonene as the dominant monoterpene isomer measured in Manhattan, which is consistent with monoterpenes observed from consumer product headspaces (*SI Appendix*, Fig. S29) and indoor environments (*SI Appendix*, Fig. S30). In contrast, α- and β-pinene were the dominant isomers in forested areas, consistent with the emissions from pine species common to northern New Jersey (22) (*SI Appendix*, Fig. S31).

In winter, monoterpenes were correlated with CO during air pollution episodes ($R^2 = 0.7$, *SI Appendix*, Fig. S5), which is likely explained by the mixing of VCPs and combustion source emissions over coincident spatial and temporal scales (8). We use this correlation, a validated CO emissions inventory, and corrections for the differences in chemical lifetime between monoterpenes and CO to estimate that anthropogenic monoterpenes were emitted at a rate of 520 to 860 mg · person^{-1} · d^{-1}. A full description of these calculations is provided in *SI Appendix*, section 6. Using measurements of fragrance formulations and inventory

estimates of fragrance emissions, we estimate that anthropogenic monoterpenes from fragranced VCPs were emitted at ~220 (±170) mg · person^{-1} · d^{-1}. Cooking and building material emissions are other possible sources of anthropogenic monoterpenes and may account for the fraction unexplained by VCPs.

The monoterpene emission rate estimated for Manhattan is significant when compared to biogenic monoterpene emissions expected for a typical US forest. For example, summertime monoterpene emissions in a dense southeast US forest are 0.40 to 0.68 kg · h^{-1} · km^{-2} or 580 to 980 kg · d^{-1} when distributed over an area the size of Manhattan (17). Total monoterpene fluxes for Manhattan, 884 to 1,462 kg · d^{-1}, are comparable to this natural source. We note that the total anthropogenic fluxes will only impact monoterpene mixing ratios on urban scales. Estimated anthropogenic monoterpene emissions from fragrance use over the entire US population (26 ± 20 kt · y^{-1} for a population of 328 million) are small compared to monoterpene emissions from US forests [9 to 37 × 10^3 kt · y^{-1} (23)].

The significant flux of anthropogenic monoterpenes, along with trends in D5-siloxane and ethanol, confirms that VOC fluxes from fragranced VCPs greatly impact the VOC burden of NYC. In *SI Appendix*, section 3, we estimate the total petrochemical mass emissions from VCPs, motor vehicles, and other fossil fuel sources following McDonald et al. (4). The speciated VOC emissions are verified with fossil fuel and VCP tracers measured by PTR-ToF-MS and GC-MS (*SI Appendix*, Fig. S10). The inventory used for NYC, termed fuel-based inventory of vehicle emissions with VCPs (FIVE-VCP), broadly explains observations of AVOCs and demonstrates that VCP emissions are ~50% (weight/weight) greater than those of fossil fuels (*SI Appendix*, Fig. S7).

Modeling Ozone during an Exceedance in NYC. During summer 2018, NYC endured a series of heat waves that led to numerous ozone exceedances (*SI Appendix*, Fig. S11). To evaluate the VCP contribution to photochemical ozone production, air quality is simulated for 5 wk (June 27 to July 31) for the continental United States, with a nested higher-resolution simulation over the Eastern United States (*SI Appendix*, Fig. S12) using the Weather Research Forecasting with Chemistry (WRF-Chem) model (see *Materials and Methods* for details). With WRF-Chem, we account for the impacts of anthropogenic and biogenic emissions on the spatial, temporal, and vertical variability of ground-level ozone in NYC. We also modify the Earth System Research Laboratory version of the Regional Atmospheric Chemistry Mechanism (RACM-ESRL) (24) used throughout this work to include the chemistry of key oxygenated molecules emitted from VCP sources (termed here as "oVCPs"). oVCP emissions are a major component of fragranced VCPs and are predominantly composed of alcohols (e.g., ethanol and isopropanol), glycols (e.g., propylene glycol and glycerol), and an array of glycol ethers. Chemical mechanisms used in modern air quality models vary in complexity and may represent reactions for smaller oxygenates such as methanol, ethanol, and ethylene glycol. It is also common for oxygenates to be lumped to hydrocarbon surrogates. For example, Qin et al. (7) recently evaluated ozone production from VCPs in Los Angeles using the SAPRC07tic mechanism, which explicitly represents methanol and ethanol but predominantly treats higher-carbon alcohols and glycols as alkanes (7, 25, 26). Oxygenates react with OH following different chemical pathways than alkanes, which may impact ozone formation and alter simulated distributions of important secondary products, such as formaldehyde, peroxyacetyl nitrate, and organic nitrates. Here, we compare the assumptions of hydrocarbon chemistry with that of oVCPs in order to evaluate the importance oVCP chemistry in the quantification of ozone and other secondary products. A full description of the mechanism updates is provided in the *SI Appendix*, section 4.2.

WRF-Chem results are shown in Fig. 3 for July 2, 2018, which was the highest ozone exceedance observed throughout the NYC area in summer 2018. A similar analysis is shown in *SI Appendix*, section 4 for the entire heat wave event (July 1 to 3; *SI Appendix*, Fig. S23) as well as for an ozone exceedance on July 16, in which the NYC outflow was transported along the Long Island Sound (*SI Appendix*, Fig. S24). We report WRF-Chem results as the maximum daily 8-h average ozone (henceforth MDA8 ozone), which is a metric used to assess ozone attainment under the Clean Air Act. Both the surface monitors (MDA8 = 115 ppb) and base-case WRF-Chem model (Fig. 3*D*, MDA8 = 114 ppb) show that peak ozone, formed downwind of NYC, reached "very unhealthy" levels according to the US air quality index (AQI). At the surface, 32 of the 39 air quality monitors located between Philadelphia, NYC, and coastal Connecticut exceeded the 70 ppb NAAQS for ozone (denoted by white circles in Fig. 3), which was also predicted by the model (36 of 39 sites). Around ~24 of 27 million people in the region were exposed to "unhealthy" air, according to the AQI.

Each panel in Fig. 3 is a WRF-Chem sensitivity analysis that illustrates the impact of VOC source sectors on ozone produced during the July 2 exceedance. Below each heading are surface ozone mixing ratios or column-integrated PAN from grid cells in Manhattan (NYC) and the ozone maximum toward the north (max). We quantify the ozone produced at the MDA8 maximum north of NYC, where the MDA8 ozone reached 115 ppb. In the following sections, we show that ozone produced until this point was formed under VOC-sensitive chemistry, in which reductions in AVOCs would likely result in the largest decrease in the ozone. Shortly downwind of this location, the ozone production transitioned to NO_x-sensitive chemistry, in which ozone reductions from decreases in NO_x outweigh the benefits of VOC reductions.

WRF-Chem simulations show that NO_x + biogenic VOCs (BVOCs) primarily contributed to NAAQS exceedances (Fig. 3*A*), which is consistent with previous observations that NO_x emissions along with BVOCs are an important contributor to regional ozone formation in the Eastern United States (27, 28). Regional background mixing ratios outside of the NYC plume result from ozone produced from the chemistry of NO_x sources upwind of NYC. At the ozone max downwind of NYC, NO_x from the NYC plume reacted alongside BVOCs to enhance ozone above the regional background to 94 ppb (a 24-ppb difference between NYC and max).

When fossil fuel VOCs are included (e.g., mobile sources and industry), modeled ozone at this location is enhanced to 102 ppb (an 8-ppb increase over ozone produced from BVOCs + NO_x; Fig. 3*B*). The addition of VCP emissions pushes this exceedance further to 113 ppb (an additional increase of 11 ppb; Fig. 3*C*). In total, AVOCs and BVOCs reacted within the NYC plume to form 43 ppb of ozone at the MDA8 max. Approximately half of this ozone is contributed from AVOC emissions. Of this anthropogenic fraction, more than 50% is attributable to VCP emissions. Similar proportions were also observed over the course of the entire heat wave event, as well as from the ozone exceedance observed on July 16 (*SI Appendix*, section 4). These analyses show that while isoprene from natural vegetation is expected to be a dominant precursor for ozone pollution in the Eastern United States (27, 28), AVOCs may significantly contribute to ozone exceedances downwind of NYC.

Fig. 3 *A*–*C* shows the impacts of AVOC emissions on ozone formation with VCPs represented in the traditional way with hydrocarbon surrogates. Fig. 3*D* shows ozone simulations when oVCPs are modeled with the inclusion of oVCP chemistry. This change in chemistry results in a small increase in ozone (1 ppb). Detailed comparisons between these two chemical representations shows that hydrocarbon chemistry reasonably approximates the ozone produced from oVCPs (*SI Appendix*, section 10). These results demonstrate that ozone in air quality models is foremost sensitive to the magnitude of VCP emissions, and reducing

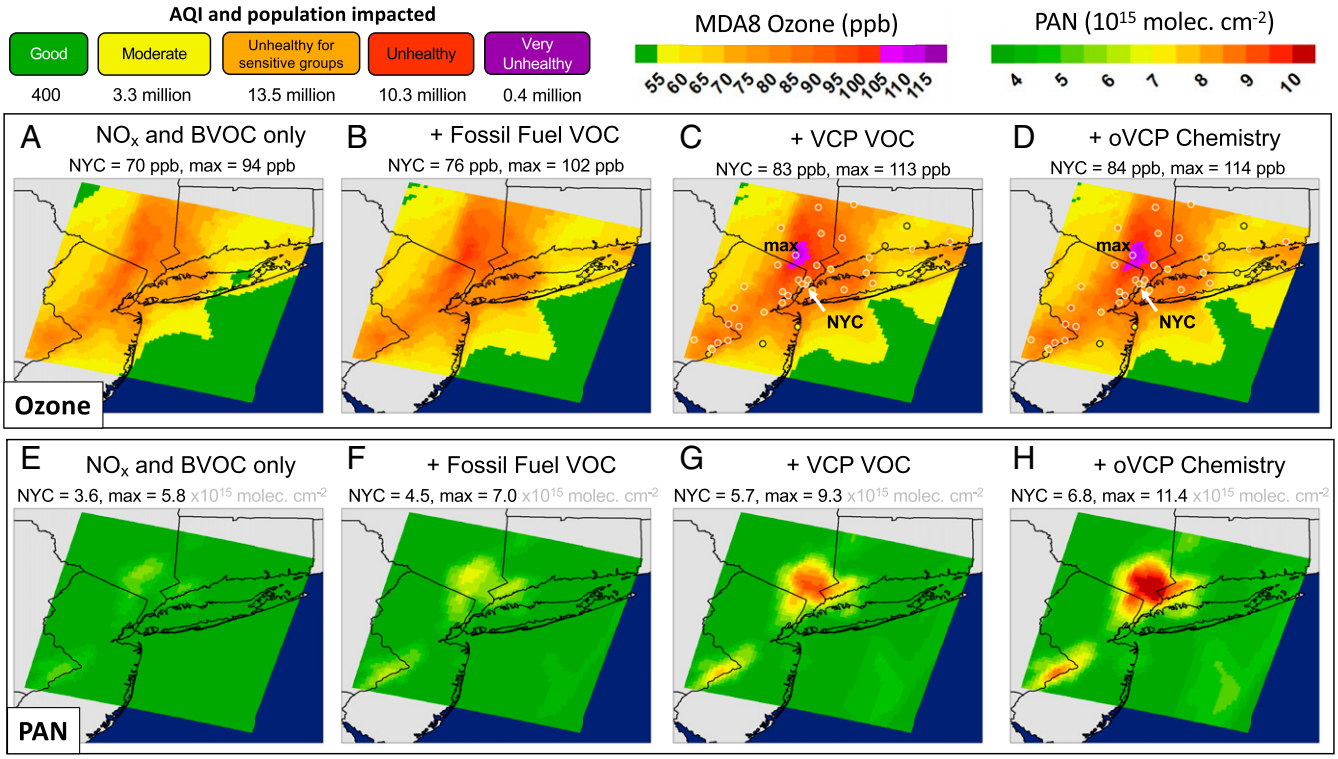

Fig. 3. WRF-Chem simulations of MDA8 ozone (parts per billion) and midday (2:00 PM local time) column integrated PAN (molecules cm^{-2}) during the July 2, 2018, pollution episode. Shown are the simulations for global background + NO_x and BVOCs (*A* and *E*), results from *A* and *E* with fossil fuel VOCs added (*B* and *F*), and results from *B* and *F* with VOCs from VCPs added (*C* and *G*). *A*–*C* and *E*–*G* show ozone and PAN produced under the assumption of hydrocarbon chemistry. *D* and *H* shows the simulation using full emissions but under the assumption of oVCP chemistry. Circles show the ozone mixing ratios measured at monitoring stations in the NYC area; those bolded in white exceeded US NAAQS. The numbers above each panel show the surface ozone or column PAN simulated in NYC and at the location of the MDA8 ozone maximum downwind of NYC (max). The US AQI, and the populations impacted within each index, are shown for reference.

uncertainties in emission inventories should be prioritized in future work.

Despite the marginal impact on the magnitude of ozone, the OH chemistry of oxygenates markedly impacts model simulations of other secondary products that have implications on downwind air quality. Oxidation of NO_x occurs simultaneously with ozone production and leads to different compound classes that serve as either permanent sinks or temporary reservoirs of NO_x. Most important among the reservoir compounds is peroxyacetyl nitrate (PAN), shown in Fig. 3 *E*–*H*. The inclusion of oVCP chemistry (Fig. 3*H*) increases PAN by 15 to 20% at the expense of organic nitrates that would otherwise permanently remove NO_x (described further in *SI Appendix*, sections 10 and 11). This shift has the potential to release NO_x from this reservoir on broader scales than those simulated here, altering the ozone production potential further downwind. These sensitivity analyses illustrate that refined chemical mechanisms are needed in order to interpret the broader impact of oVCPs on urban atmospheric chemistry.

SI Appendix, Fig. S40 shows a similar analysis for formaldehyde. Formaldehyde is measured from space, and its ratio to NO_2 is used to infer ozone sensitivities to VOCs and NO_x (29, 30). WRF-Chem shows that formaldehyde is dominated by the chemistry of biogenic isoprene, followed by light alkenes emitted from tailpipe exhaust (described further in *SI Appendix*, section 11). The contributions from VCP emissions are smaller than those from fossil fuels, and the inclusion of oVCP chemistry results in modest increases.

Our modeling suggests that formaldehyde production is most sensitive to the chemistry of hydrocarbons, whereas PAN is more sensitive to the chemistry of oxygenates. In the following discussion, we show that oxygenates are a major contributor to ozone derived from VCPs. Consequently, future studies may benefit from leveraging observations of PAN in conjunction with formaldehyde to better constrain ozone responses to fossil fuel and VCP emissions.

Attribution of Ozone Produced from VCPs. To complement the WRF-Chem modeling, we constructed a Lagrangian box model to further evaluate the chemical processes impacting air quality in the NYC region. The model is initialized at 11:00 AM on July 2, 2018, to simulate the NYC plume after the mixed layer has developed. The box model employs the updated oVCP chemistry used in WRF-Chem and is initialized with the midday emissions estimated for Manhattan. Since personal care products are predominantly emitted before 11:00 AM (*SI Appendix*, Fig. S27), the consumer product emissions used to initialize the box model are disproportionately lower than those represented in the FIVE-VCP inventory and WRF-Chem modeling across the whole day. A full description of the box model and comparison to WRF-Chem trajectories is provided in *SI Appendix*, section 5.

We evaluate the contributions of AVOCs to downwind ozone by conducting VOC sensitivity analyses for each of the ~1,600 species in the FIVE-VCP inventory. Fig. 4 summarizes the distribution of box model emissions, the resulting ozone produced from AVOCs, and the emission sector ozone yields calculated at the location of the MD8A ozone max downwind of NYC. Total ozone is the product of emissions, the percentage of VOCs that react during transport to the MDA8 ozone maximum (shown in parenthesis), and the ozone yields.

Fossil fuel emissions are most efficient in producing ozone and account for ~60% of the AVOC-derived ozone produced at midday by the box model analysis. VCP sectors have lower ozone yields but significantly higher mass emissions (~50% greater), which results in comparable ozone formation. Fragranced and nonfragranced VCPs contribute equally to downwind ozone, with the dominant sectors being coatings, adhesives, personal care, and cleaning. Among all VCP emissions, monoterpenes, ethanol, and oxygenates, which predominantly result from fragranced VCPs, constitute ~50% of the VCP-produced ozone. The remaining fraction is attributable to aromatics and alkanes emitted from coatings and adhesives.

Fig. 4 shows that both emissions and ozone yield are important in determining the distribution of AVOC ozone. Ozone yields from gasoline are highest (~2.4 g/g) because of the significant fraction of alkyl aromatics and alkenes, which are known to be very efficient ozone precursors (31). Oxygenates are less efficient at producing ozone (31) and have been added to consumer VCPs as replacements for more reactive hydrocarbons (21). Glycols are a dominant component of oxygenate emissions and reactivity (*SI Appendix*, Fig. S35) but are typically exempt from regulations based on limits imposed on ingredient volatility and ozone formation potential (21). While these oxygenated components may produce less ozone per gram emitted as intended, our modeling suggests that the extensive use of these ingredients in consumer product formulations still leads to significant ozone formation.

Ozone Sensitivity to VOC and NO_x Reductions. Ozone mitigation strategies in urban regions often emphasize controls on NO_x, though VCPs are also regulated for their impacts on ozone (32). Based on WRF-Chem simulations, ozone formation downwind of NYC was partly sensitive to AVOC emissions. Fig. 5 shows changes in ozone when box model emissions of NO_x and AVOCs are reduced by 50%. Model output is shown along the NYC plume trajectory (shown here as distance from Central Park), and the background colors indicate when ozone production transitions from VOC to NO_x-sensitive chemistry. A 50% decrease in AVOCs had the greatest impact on ozone formation within 40 km of Manhattan, where ozone production rates were largely VOC sensitive. In contrast, a 50% decrease in NO_x resulted in lower ozone formation on a regional scale (>40 km from Central Park) following a transition to NO_x-sensitive ozone production. The population density along the plume trajectory shows that on July 2, most people exposed to the ozone exceedance resided in regions likely to be sensitive to local AVOC reductions.

It is expected that continued NO_x reductions will result in reduced, plume-averaged ozone pollution for cities across the United States (6). The results presented in Fig. 5 supports these conclusions for ozone production at regional scales; however, in NYC, a large fraction of the population was exposed to elevated ozone mixing ratios that were produced under VOC-limited conditions. It is notable that the local ozone production rate was VOC-limited, even though NYC is surrounded by an isoprene-rich environment. VOC-sensitive ozone production may play a role in other megacities, especially those in semiarid regions where regional biogenic emissions are lower (e.g., Los Angeles). VCPs contribute to ozone in these regions (4, 7), and the results for NYC show that VPCs can affect ozone processes in megacities with broader VOC emission sources.

While the July 2 exceedance represents a case study of ozone formed during a heat wave, it is expected that similar extreme heat events will become more frequent in a warming climate (33). Such events already contribute significantly to the number of ozone exceedances observed in urban areas, especially in the Eastern United States (33, 34). Ozone mitigation strategies may benefit from considering the combined impacts of NO_x and VOC reductions on local and regional scales, as well as how these changes impact ozone production during extreme heat events.

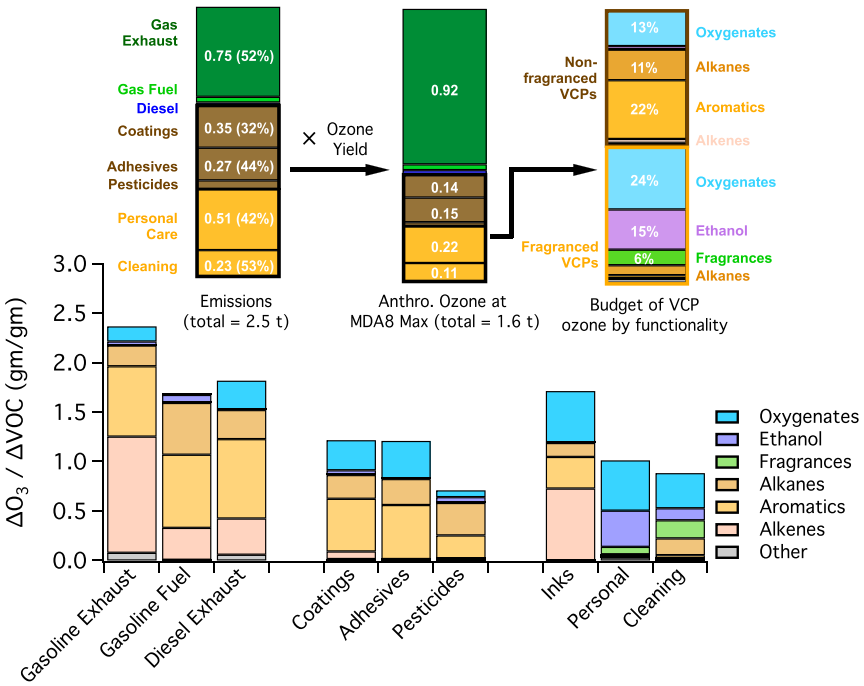

Fig. 4. Budget of AVOC contributions to ozone produced at the MDA8 ozone max of NYC (Fig. 3). The flow chart shows that the total emissions added to the box model, followed by the ozone produced by emission sector and chemical functionality. The numbers in the parenthesis represent the percentage of the VOCs that reacted before the plume reached the MDA8 ozone maximum. The bar chart shows the yield of ozone (gram/gram) produced from fossil fuel sources, nonfragranced VCPs (coatings, adhesives, and pesticides), and fragranced VCPs (inks, personal care, and cleaning). Each bar is colored to show the fraction of ozone produced within each sector by different chemical classes.

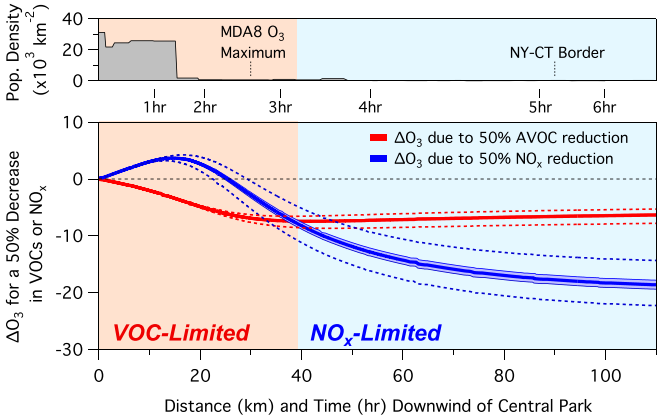

Fig. 5. Calculated change in ozone downwind of NYC, assuming a 50% decrease in NO_x or VOCs. The population density along the plume transit is shown to highlight urban areas impacted by VOC or NO_x-limited ozone formation. Shaded regions delineate where the ozone isopleth transitions from VOC-limited ($dO_3/dNO_x < 0$) to NO_x-limited ($dO_3/dNO_x > 0$). Error bands show the model results, assuming 10% (solid bands) and 50% (dotted lines) changes to isoprene mixing ratios (base case 0.75 ppb). NY-CT, New York–Connecticut.

VCP emissions compose a significant fraction of ozone produced from AVOC sources and represent a mitigation lever that is decoupled from NO_x emission sources. VCPs are prevalent across the United States and Europe and may impact the air quality of other megacities around the world experiencing significant ozone pollution.

Materials and Methods

Ground Site Measurements and 2018 Long Island Sound Tropospheric Ozone Study Campaign Description. The New York Investigation of Consumer Emissions (NY-ICE) was a 2-mo field campaign conducted in winter (March 5 to 28, 2018) and summer (July 5 to 24, 2018) to measure the emission profile and strength of VOCs emitted from VCPs. The sampling periods were chosen in order to study VCP emissions during periods with both low-biogenic activity (winter) and high potential for ozone pollution (summer). Measurements conducted in the summer were performed as part of the 2018 Long Island Sound Tropospheric Ozone Study (LISTOS 2018, https://www.nescaum.org/documents/listos#about), which was a multiagency field initiative aimed at understanding the influence of NYC emissions on ozone formation and transport along the New England coast.

VOC and CO mixing ratios were measured from an engineering building located at the CCNY. During winter, instruments were placed in a basement and sampled air at the top of a roof through a 10-m Teflon inlet. The total flow through the inlet was 15 L · min^{-1}, and line losses for species reported here were negligible. In summer, the instruments were staged at the top of the building and sampled air through a 1-m Teflon inlet. Measurements were conducted for at least 2 wk to characterize VOC temporal profiles and VOC/CO ERs.

Instrumentation. VOC mixing ratios were measured using a PTR-ToF-MS (Tofwerk AG) and a custom-built whole air canister system (WAS) analyzed by GC-MS (WAS-GC-MS) (35, 36). The PTR-ToF-MS is sensitive to a broad range of VOCs, including aromatics, alkenes, biogenic species, and oxygenates. Reported here are measurements of benzene, the sum of monoterpenes, and D5-siloxane, as well as a suite of other VOCs representative of biogenic and anthropogenic sources. The WAS-GC-MS provides information about VOC isomers, which cannot be resolved by the PTR-ToF-MS. WAS-GC-MS measurements are primarily used to evaluate monoterpene distributions, determine mixing ratios of alkane hydrocarbons, and verify compound-specific identities attributed to the masses measured by the PTR-TOF-MS.

During ground site sampling, PTR-ToF-MS backgrounds were determined in situ every 2 h by passing air through a platinum catalyst heated to 350 °C. During drives, instrument backgrounds were determined every 15 min. Data were processed following the recommendations of Stark et al. (37) using the Tofware package in Igor Pro (WaveMetrics).

The WAS sampling system consists of a stainless steel bellow compressor, 12 to 24 canisters in series, a pneumatics system, and computer control (35). Each 2.7 L electropolished stainless steel canister is initially cleaned, evacuated, and filled to 10 Torr water vapor before shipping to the field (2). Canister samples were automatically collected every 2 h during ground site measurements and manually triggered during mobile drives. During sampling, each evacuated canister is opened electronically by pneumatically actuated stainless steel bellows valves on each canister. The compressor is upstream of the samplers and is used to pressurize each canister to ~45 psig. The compressor was intentionally throttled down so that the average fill time was over 5 min in order to reduce the impacts of local, intermittent plumes. For winter 2018, 126 mobile and 207 stationary canisters were collected. During summer 2018, 37 mobile and 141 stationary samples were collected. The canisters were shipped back to Boulder, CO, and analyzed by the GC-MS within 4 d of collection to minimize sampling artifacts. Sampling artifacts, because of VOC canister storage, have been characterized previously and are expected to be negligible for the species reported here (35). WAS-GC-MS instrument backgrounds were characterized by filling cleaned canisters with ultrapure nitrogen (Matheson, Inc.) and analyzing on the GC-MS.

Each canister sample is analyzed on a custom, two-channel GC-MS with a duty cycle of 20 min per sample. Two separate 240 mL aliquots are collected from each canister sample simultaneously and analyzed in series using a single quadrupole mass spectrometer (Agilent 5975C) operated in selected ion monitoring/scan mode. Channel 1 consists of a CO_2 trap (Ascarite II, Thomas Scientific), water trap at −55 °C, and a sample preconcentration trap at −165 °C coupled to an Al_2O_3-KCL porous layer open tubular column (Restek RT-Alumina bonded porous polymer/KCl; 30-m length × 0.25-mm inner diameter [ID], and 4-μm film thickness) designed to separate the C2 to C6 hydrocarbons and select halocarbons. Channel 2 consists of a water trap at −55 °C and a sample preconcentration trap at −155 °C coupled to a DB-624 column (Restek MXT-624; 30-m length × 0.25-mm ID, 1.4-μm film thickness) designed to separate the C5 to C12 hydrocarbons and select oxygen-, halogen-, and nitrogen-containing VOCs.

VOC mixing ratios in Europe were measured using a Vocus S PTR-ToF-MS (Tofwerk AG). Ambient air was sampled at a flow rate of 5 L · min^{-1} through a 2-m-long, 1/8″ ID PFA inlet mounted above the engine. Instrument background was determined at the beginning of the drive and thereafter for select compounds by 30 s zero performed every 20 min by passing air through an activated charcoal filter. Single-point calibrations were performed approximately every 2 h.

The NOAA PTR-ToF-MS and WAS-GC-MS were calibrated using multiple, gravimetrically prepared gas standards and by liquid calibration methods, as described by Coggon et al. (8). The Tofwerk PTR-ToF-MS was calibrated using an onboard, gravimetrically prepared gas standard. Instrument sensitivities and data intercomparisons are provided in *SI Appendix*, section 2.

CO was measured from the NYC ground site and onboard the NOAA mobile laboratory by integrated cavity output spectroscopy (Los Gatos Research, Inc.). The CO monitor was calibrated using certified CO in-air standards (Scott-Marrin, Inc), which in turn were calibrated before and after the project to standards on the WMO CO_X2014A scale. Other instruments deployed during LISTOS 2018 are described in *SI Appendix*, section 4.

Mobile Measurements and Urban Enhancement Ratio Calculations. Mobile measurements were conducted in NYC and other US cities onboard the NOAA mobile laboratory (38, 39) to characterize the spatial distribution of VCP emissions. In NYC, the mobile laboratory was driven through the NYC metropolitan area, including Long Island and northeastern New Jersey (*SI Appendix*, Fig. S1). The drive paths were designed to sample regions of high- and low-population density to compare differences in VCP emissions. The mobile laboratory was also driven through forested regions of New Jersey and Long Island in order to contrast natural monoterpene emissions with those of fragranced VCPs.

At the beginning and end of each deployment, the mobile laboratory was driven across the United States to sample urban emissions from other cities, as well as to characterize rural emissions of isoprene. Detailed mobile sampling was conducted for Denver, CO; Chicago, IL; and Pittsburgh, PA. For each city, urban emissions were characterized by sampling VOCs along surface roads and in densely populated regions, such as city centers. Urban emissions were contrasted with measurements in suburban and rural regions upwind and downwind of each city. Here, we focus on morning measurements (8:00 AM to 12:00 PM local time), when VCP emissions are expected to be highest. Multiple drives were conducted in NYC (three), Denver (two), and Chicago (two), while one was conducted for Pittsburgh. The trends in population

density shown in Fig. 2 were measured over two separate drives and were similar to other drives conducted during summer.

VOC measurements in Europe were conducted onboard the Tofwerk mobile laboratory using a PTR-ToF-MS. Drives were conducted September 24 to 25, 2019, from Thun, Switzerland, past Bratislava, Slovakia. In contrast to the US sampling strategy, measurements in Europe were performed exclusively on the highway. Urban emissions were sampled in close proximity to multiple cities (*SI Appendix*, Fig. S2); however, only Bratislava, Bern, and Vienna were sampled through dense population centers during morning hours. These cities are analyzed in detail to compare to US-based observations.

In this study, we evaluate VOC/benzene ERs in US and European cities in order to compare VCP and traffic emissions across urban regions with different population densities. We calculate urban VOC/benzene ERs as described in Eq. **1**.

$$\mathrm{ER} = \frac{[\mathrm{VOC}]_{\text{median in city}} - [\mathrm{VOC}]_{\text{median out of city}}}{[\mathrm{Benzene}]_{\text{median in city}} - [\mathrm{Benzene}]_{\text{median out of city}}}. \quad [1]$$

We calculate ERs using median mixing ratios in order to screen for enhancements due to short, localized plumes commonly measured by mobile laboratory. Morning hour median mixing ratios were calculated from measurements conducted in the population center of each city and from upwind measurements, where VCP and traffic emissions were expected to be low. NYC has large differences in population density across the five boroughs; consequently, NYC measurements are separated based on measurements conducted in areas of high- (19,000 to 23,000 people $\cdot$ km^{-2}), medium- (14,000 to 19,000 people $\cdot$ km^{-2}), and low- (9,000 to 14,000 people $\cdot$ km^{-2}) population densities.

WRF-Chem and Box Model Descriptions. In this study, we utilize a three-dimensional (3D) chemical transport model to quantify ozone observed during the 2018 ozone season and a complementary Lagrangian box model to assess the influence of AVOC emissions on ozone exceedances in the Long Island Sound region. The 3D model employs the WRF-Chem model, in which chemistry is fully coupled with meteorology (40). The box model employs the same chemical mechanism and emissions inventory as WRF-Chem but is parameterized to use simplified meteorology in order to facilitate solver efficiency.

WRF-Chem. A full description of the WRF-Chem and box model, and comparison to instrumentation deployed during LISTOS 2018, is provided in the *SI Appendix*. Briefly, we use WRF-Chem version 4.0 to simulate the Continental United States at 12 $\times$ 12 km horizontal resolution with 50 vertical levels (up to 50 hPa). The continental run provides initial and boundary conditions for the nested Eastern US domain at 4 $\times$ 4 km horizontal resolution. We make the nested domain sufficiently large to reduce potential effects of complex terrain, due to the Appalachian Mountains, on our nested meteorological simulations. Air quality is simulated from June 25 to July 31, 2018, to assess the highest ozone exceedances observed during summer 2018, as well as to overlap with LISTOS 2018 measurements.

We initialize meteorology with the North American Mesoscale model and utilize the Noah Land Surface Model and Mellor–Yamada–Nakanishi and Niino planetary boundary layer scheme. BVOC emissions are based on the Model of Emissions of Gases and Aerosols from Nature model, version 2.1 (41), with adjusted isoprene emissions based on mobile van measurements, as described in *SI Appendix*, section 4.

Anthropogenic CO, NO_x, and VOC emissions are from an emissions inventory developed for the continental United States and NYC. The FIVE-VCP inventory was developed following the methods described by McDonald et al. (4, 42). The emissions inventory is compared to VOC/CO ratios measured at the CCNY ground site during summer and winter. A full description of the inventory, as well as a comparison to the ground site measurements, is provided in *SI Appendix*, section 3.

Finally, we represent the atmospheric chemistry of NO_x, VOCs, and ozone using the Madronich Photolysis (Tropospheric Ultraviolet and Visible) scheme and RACM-ESRL chemical mechanism described by Kim et al. (43) with modifications to include the chemistry of key oVCPs, including ethanol, methanol, isopropanol, acetone, propylene glycol, ethylene glycol, and glycerol. Often, oVCP emissions are treated as hydrocarbon surrogates in air quality models, which likely misrepresents the atmospheric chemistry of oVCP emissions. While several reduced chemical mechanisms include acetone, ethanol, and methanol, few include surrogates for glycols or glycerol. We conduct sensitivity analyses to explore the extent to which the assumption of hydrocarbon or oVCP chemistry impacts the production of ozone from oVCP emissions and also consider how these mechanistic differences impact the formation of other key secondary pollutants, such as formaldehyde, peroxyacetyl nitrate, and alkyl nitrates. Details describing the updates made to RACM-ESRL are provided in *SI Appendix*, section 4.2, and the implications of this chemistry are detailed in *SI Appendix*, sections 9–12.

The WRF-Chem simulations are extensively compared to ground site and mobile laboratory measurements of key chemical species (isoprene, formaldehyde, NO_2, and ozone) and meteorological parameters (planetary boundary layer height, horizontal wind speed and direction, and vertical ozone structure) and describe these observations to within 10%. We also compare model simulations against University of Maryland aircraft measurements of CO, ozone, and NO_2 conducted during the July 1 to 2, 2018 heat wave. The model agrees to within 20% for CO and NO_2 and describes the highest ozone observations to within 10 ppb. Details describing these comparisons are provided in *SI Appendix*, section 4.

Box model. The box model is constructed using the Framework for 0-D Atmospheric Modeling (44). The model is set up to treat the outflow from NYC as a Lagrangian plume in order to assess the impacts of NYC pollution on downwind ozone formation. We focus the box model analysis on July 2, 2018, which was the highest ozone exceedance observed during summer 2018 (MDA8 ozone exceeded 100 ppb in Manhattan and over 120 ppb downwind).

The volume of the box is assumed to be equivalent to the area of Manhattan (~60 km^2) and the height of the planetary boundary layer (~1.2 km). Advection and dilution in the box are constrained based on WRF-Chem output of CO along the Lagrangian trajectories of air masses originating from Manhattan. The box model is run between 11:00 AM and 5:00 PM, when the height of the planetary boundary layer has stabilized, as measured by light detection and ranging (LIDAR) from the CCNY ground site. Emissions from the FIVE-VCP inventory are used to initialize VOC and NO_x mixing ratios. We account for the diurnal pattern of fossil fuel and VCPs by scaling emissions to those expected for 11:00 AM. Consumer product emissions are predominantly emitted during morning hours and are disproportionately lower than those represented by WRF-Chem over the entire day. Initial NO_x emissions are partitioned to NO and NO_2, assuming that both species are at pseudosteady state with ozone. Isoprene concentrations are constrained based on mobile laboratory drives across the NYC metropolitan area (~0.75 ppb, *SI Appendix*, Fig. S17). Additional analyses are conducted to evaluate model sensitivity to biogenic emissions by varying the isoprene constraint by 10 and 50%.

The output from the box model is compared to trajectory output from WRF-Chem during the July 2, 2018 ozone episode. The temporal evolution of chemical species between the two models agree to within 30%. A full description of the model and comparison to WRF-Chem is provided in *SI Appendix*, section 5.

Data Availability. Data for LISTOS, University of Maryland Aircraft, and Pandora spectrometers can be accessed through the NASA data archive. Data for the NOAA mobile laboratory, NY-ICE, and LISTOS measurement campaigns can be found at the can be found at the NOAA Chemical Sciences Laboratory measurement website. Emission files used to initiate WRF-Chem and box model simulations are also available at the CSL website. Data have been deposited in the NASA archive (https://www-air.larc.nasa.gov/missions/listos/index.html) and CSL archive (https://www.esrl.noaa.gov/csd/groups/csd7/measurements/2018nyice/).

ACKNOWLEDGMENTS. We thank Andrew Whitehill for useful comments to the manuscript and permission to use formaldehyde data collected during LISTOS. We thank Lukas Valin, James Szykman, and David Williams for insightful discussions and permission to use the Pandora data collected during LISTOS. We thank the NASA Pandora Project team for logistical and calibration support (led by R. Swap, L. Shalaby, A. Dimov, A. Suliman, A. Kotsakis, and F. Santos) and the Luftblick Pandonia team for calibration and data processing support (led by A. Cede, M. Tiefengraber, M. Mueller, and M. Gebetsberger). We thank Paul Miller for coordinating LISTOS and logistical support. We thank Albert Presto and Rishabh Shah for ground support during measurements in Pittsburgh, PA. M.M.C., G.I.G., B.C.M., M.L., S.A.M., J.P., and C.W. acknowledge the Cooperative Institute for Research in Environmental Sciences (CIRES) cooperative agreement NA17OAR4320101. M.M.C., G.I.G., B.C.M., M.L., and R.S. acknowledge support through the Environmental Protection Agency's Science to Achieve Results Program Grant 84001001. M.M.C., G.I.G., J.B.G., B.C.M., and C.W. acknowledge the CIRES Innovative Research Program. F.M., M.A., and Y.W. acknowledge the NOAA Cooperative Science Center for Earth System Sciences and Remote Sensing Technologies under the Cooperative Agreement Grant NA16SEC4810008 and Northeast States for Coordinated Air Use Management Project 2411. T.B. and G.G. acknowledge supplemental funding from the NASA Tropospheric Composition Program. X.R. and R.D. acknowledge supplemental funding from the National Institute for Standards and Technology. A.W. acknowledges the NOAA Hollings Scholar Program.

1. I. B. Pollack *et al*., Trends in ozone, its precursors, and related secondary oxidation products in Los Angeles, California: A synthesis of measurements from 1960 to 2010. *J. Geophys. Res. Atmos.* **118**, 5893–5911 (2013).
2. Z. Jiang *et al*., Unexpected slowdown of US pollutant emission reduction in the past decade. *Proc. Natl. Acad. Sci. U.S.A.* **115**, 5099–5104 (2018).
3. C. Warneke *et al*., Multiyear trends in volatile organic compounds in Los Angeles, California: Five decades of decreasing emissions. *J. Geophys. Res.*, 10.1029/2012JD017899 (2012).
4. B. C. McDonald *et al*., Volatile chemical products emerging as largest petrochemical source of urban organic emissions. *Science* **359**, 760–764 (2018).
5. A. Gaudel *et al*., Aircraft observations since the 1990s reveal increases of tropospheric ozone at multiple locations across the Northern Hemisphere. *Sci. Adv.* **6**, eaba8272 (2020).
6. J. L. Laughner, R. C. Cohen, Direct observation of changing NO_x lifetime in North American cities. *Science* **366**, 723–727 (2019).
7. M. Qin *et al*., Criteria pollutant impacts of volatile chemical products informed by near-field modeling. *Nat. Sustain.*, 129–137 (2020).
8. M. M. Coggon *et al*., Diurnal variability and emission pattern of decamethylcyclopentasiloxane (D_5) from the application of personal care products in two North American cities. *Environ. Sci. Technol.* **52**, 5610–5618 (2018).
9. L. M. Bettencourt, J. Lobo, D. Helbing, C. Kühnert, G. B. West, Growth, innovation, scaling, and the pace of life in cities. *Proc. Natl. Acad. Sci. U.S.A.* **104**, 7301–7306 (2007).
10. C. K. Gately, L. R. Hutyra, I. Sue Wing, Cities, traffic, and CO_2: A multidecadal assessment of trends, drivers, and scaling relationships. *Proc. Natl. Acad. Sci. U.S.A.* **112**, 4999–5004 (2015).
11. L. N. Lamsal, R. V. Martin, D. D. Parrish, N. A. Krotkov, Scaling relationship for NO_2 pollution and urban population size: A satellite perspective. *Environ. Sci. Technol.* **47**, 7855–7861 (2013).
12. G. I. Gkatzelis *et al*., Identifying volatile chemical product tracer compounds in U.S. cities. *Environ. Sci. Technol.* **55**, 188–199 (2021).
13. D. Mackay *et al*., Decamethylcyclopentasiloxane (D5) environmental sources, fate, transport, and routes of exposure. *Environ. Toxicol. Chem.* **34**, 2689–2702 (2015).
14. M. W. Alton, E. C. Browne, Atmospheric chemistry of volatile methyl siloxanes: Kinetics and products of oxidation by OH radicals and Cl atoms. *Environ. Sci. Technol.* **54**, 5992–5999 (2020).
15. M. S. McLachlan *et al*., Concentrations and fate of decamethylcyclopentasiloxane (D(5)) in the atmosphere. *Environ. Sci. Technol.* **44**, 5365–5370 (2010).
16. J. A. de Gouw *et al*., Increasing atmospheric burden of ethanol in the United States. *Geophys. Res. Lett.*, 10.1029/2012GL052109 (2012).
17. C. Warneke *et al*., Biogenic emission measurement and inventories determination of biogenic emissions in the eastern United States and Texas and comparison with biogenic emission inventories. *J. Geophys. Res.* **115**, D00F18 (2010).
18. J. M. Logue, T. E. McKone, M. H. Sherman, B. C. Singer, Hazard assessment of chemical air contaminants measured in residences. *Indoor Air* **21**, 92–109 (2011).
19. A. Steinemann, Volatile emissions from common consumer products. *Air Qual. Atmos. Health* **8**, 273–281 (2015).
20. A. C. Steinemann *et al*., Fragranced consumer products: Chemicals emitted, ingredients unlisted. *Environ. Impact Assess.* **31**, 328–333 (2011).
21. CARB, "2013-2015 Consumer and commercial products survey" (California Air Resources Board, Sacramento, CA, 2019).
22. C. Geron, R. R. Rasmussen, R. Arnts, A. Guenther, A review and synthesis of monoterpene speciation from forests in the United States. *Atmos. Environ.* **34**, 1761–1781 (2000).
23. A. Guenther *et al*., A global model of natural volatile organic compound emissions. *J. Geophys. Res. D Atmospheres* **100**, 8873–8892 (1995).
24. S.-W. Kim *et al*., Modeling the weekly cycle of NOx and CO emissions and their impacts on O_3 in the Los Angeles-South Coast Air Basin during the CalNex 2010 field campaign. *J. Geophys. Res. D Atmospheres* **121**, 1340–1360 (2016).
25. W. P. L. Carter, Development of the SAPRC-07 chemical mechanism. *Atmos. Environ.* **44**, 5324–5335 (2010).
26. Y. Xie *et al*., Understanding the impact of recent advances in isoprene photooxidation on simulations of regional air quality. *Atmos. Chem. Phys.* **13**, 8439–8455 (2013).
27. W. L. Chameides, R. W. Lindsay, J. Richardson, C. S. Kiang, The role of biogenic hydrocarbons in urban photochemical smog: Atlanta as a case study. *Science* **241**, 1473–1475 (1988).
28. M. Trainer *et al*., Models and observations of the impact of natural hydrocarbons on rural ozone. *Nature* **392**, 705–707 (1987).
29. B. N. Duncan *et al*., Application of OMI observations to a space-based indicator of NOx and VOC controls on surface ozone formation. *Atmos. Environ.* **44**, 2213–2223 (2010).
30. X. Jin, A. Fiore, K. F. Boersma, I. Smedt, L. Valin, Inferring changes in summertime surface ozone-NO_x-VOC chemistry over U.S. urban areas from two decades of satellite and ground-based observations. *Environ. Sci. Technol.* **54**, 6518–6529 (2020).
31. W. Carter, "Updated Maximum Incremental Reactivity Scale and Hydrocarbon Bin Reactivities for Regulatory Applications" (Tech. Rep. California Air Resources Board Contract 07-339, University of California, Riverside, CA, 2010).
32. EPA, "Study of volatile organic compound emissions from consumer and commercial products" (EPA-453/R-94-066-A, US Environmental Protection Agency, 1995).
33. D. J. Jacob, D. A. Winner, Effect of climate change on air quality. *Atmos. Environ.* **43**, 51–63 (2009).
34. L. Shen, L. J. Mickley, E. Gilleland, Impact of increasing heat waves on U.S. ozone episodes in the 2050s: Results from a multimodel analysis using extreme value theory. *Geophys. Res. Lett.* **43**, 4017–4025 (2016).
35. B. M. Lerner *et al*., An improved, automated whole air sampler and gas chromatography mass spectrometry analysis system for volatile organic compounds in the atmosphere. *Atmos. Meas. Tech.* **10**, 291–313 (2017).
36. B. Yuan *et al*., A high-resolution time-of-flight chemical ionization mass spectrometer utilizing hydronium ions (H_3O+ToF-CIMS) for measurements of volatile organic compounds in the atmosphere. *Atmos. Meas. Tech.* **9**, 2735–2752 (2016).
37. H. Stark *et al*., Methods to extract molecular and bulk chemical information from series of complex mass spectra with limited mass resolution. *Int. J. Mass Spectrom.* **389**, 26–38 (2015).
38. M. M. Coggon *et al*., Emissions of nitrogen-containing organic compounds from the burning of herbaceous and arboraceous biomass: Fuel composition dependence and the variability of commonly used nitrile tracers. *Geophys. Res. Lett.* **43**, 9903–9912 (2016).
39. B. Yuan *et al*., Emissions of volatile organic compounds (VOCs) from concentrated animal feeding operations (CAFOs): Chemical compositions and separation of sources. *Atmos. Chem. Phys.* **17**, 4945–4956 (2017).
40. G. A. Grell *et al*., Fully coupled "online" chemistry within the WRF model. *Atmos. Environ.* **39**, 6957–6975 (2005).
41. A. Guenther *et al*., Estimates of global terrestrial isoprene emissions using MEGAN (Model of Emissions of Gases and Aerosols from Nature). *Atmos. Chem. Phys.* **6**, 3181–3210 (2006).
42. B. C. McDonald *et al*., Modeling Ozone in the Eastern U.S. using a fuel-based mobile source emissions inventory. *Environ. Sci. Technol.* **52**, 7360–7370 (2018).
43. S.-W. Kim *et al*., NO_2 columns in the western United States observed from space and simulated by a regional chemistry model and their implications for NOx emissions. *J. Geophys. Res.*, 10.1029/2008JD011343 (2009).
44. G. M. Wolfe, M. R. Marvin, S. J. Roberts, K. R. Travis, J. Liao, The framework for 0-D atmospheric modeling (F0AM) v3.1. *Geosci. Model Dev.* **9**, 3309–3319 (2016).